Comparison of 3D Accuracy of Conventional Cast Metal to Milled Zirconia Implant-Supported Full-Arch Fixed Dental Prosthesis Frameworks

Eunice Siew Pei Lua, BDS, MDS[1]/Keson Beng Choon Tan, BDS, MSD[1]/Frank Kong Fei Lee, BDS, MDS[1]/
Sophia Hui Xin Yee, BDS, MDS[2]/Keng Mun Wong, BDS, MSD[1]/Ming Yi Tan, BDS, MDS[1]

Purpose: To compare the 3D accuracy of conventional and digital workflows in the fabrication of implant-supported full-arch fixed dental prosthesis (FAFDP) frameworks for an edentulous mandible. ***Materials and Methods:*** A heat-polymerized polymethyl methacrylate (PMMA) master model simulated an edentulous mandible to be restored with a fixed prosthesis supported by five implants (implants A to E). A conventional open-tray, splinted-coping polyether impression was poured with type 4 dental stone to produce a stone model, which was scanned with a dental laboratory scanner to produce a virtual model. Zirconia (Zr) full-contour (ZFC) (n = 5) and Zr cutback (ZCB) (n = 5) frameworks were fabricated with CAD/CAM. The stone model was used as a working model to fabricate conventional noble metal frameworks (CNB) (n = 5). Each test framework was attached to five implants with application of 35-Ncm torque. Test models were fabricated with type 4 dental stone and were allowed to set completely before removing the test frameworks. Centroid positions and central axes of the implants in master and test models were measured with a coordinate measuring machine and compared. The local coordinate system comprised implant A (right posterior implant) as the origin; implants A, C (central incisor implant), and E (left posterior implant) as the xy-plane; and implants A and E as the x-axis. Three linear distortion parameters (d_x, d_y, and d_z), one global linear distortion parameter (d_R), two angular distortion parameters ($d\theta_x$ and $d\theta_y$), and 3D distance distortion values (ΔR and %ΔR) were assessed. ***Results:*** The magnitude of mean d_x, d_y, d_z, and d_R values ranged from 39.9 ± 26.4 μm (CNB-B) to 263.3 ± 94.6 μm (CNB-E) for d_x; from 56.9 ± 5.4 μm (ZFC-B) to 124.5 ± 37.6 μm (ZCB-C) for d_y; from −8.3 ± 27.6 μm (ZFC-D) to −24.6 ± 17.3 μm (ZCB-D) for d_z; and from 80.6 ± 29.4 μm (CNB-B) to 263.3 ± 94.6 μm (CNB-E) for d_R. The magnitude of mean $d\theta_x$ and $d\theta_y$ ranged from 0.025 ± 0.486 degrees (ZFC-C) to 1.490 ± 0.383 degrees (CNB-C) and from −0.050 ± 0.171 degrees (ZCB-B) to 1.263 ± 0.501 degrees (ZFC-C), respectively. One-way analysis of variance (ANOVA) found differences among groups for d_x, d_y, d_z, $d\theta_x$, and $d\theta_y$ at some implants, but there was no clear pattern on the poorest group. For global linear distortion (d_R), CNB-D fared the worst. However, CNB exhibited the worst accuracy in ΔR and %ΔR for all reference distances, except implant A to implant E. ***Conclusions:*** There were no differences between ZFC and ZCB for all parameters. CNB fared poorest for ΔR and %ΔR for three of the four reference distances (A-B, A-C, and A-D), as well as for dR for one of five implant positions (implant D). *Int J Oral Maxillofac Implants 2026;41:53–60. doi: 10.11607/jomi.11262*

Keywords: CAD/CAM, coordinate measuring machine, implant prosthodontics, 3D accuracy

The assessment of misfit in an implant full-arch fixed dental prosthesis (FAFDP) and its potential influence on biologic and mechanical complications is difficult to define. There is currently no consensus on what constitutes passive fit, although its importance is undisputed.[1]

Distortion can occur at any step of the conventional fabrication workflow, including impression making, implant component positioning, master cast fabrication, wax pattern fabrication, investment and casting, and ceramic firing. These errors are mostly due to volumetric inconsistencies and linear expansions or shrinkages of materials used.[2] The cumulative effect of distortions at various clinical or laboratory steps can result in significant strains within the bone, implant, and prosthesis assembly.[3,4] This may trigger mechanical complications and compromise the biologic integrity of the bone-implant interface.[5] Mechanical complications include loosening or even fracture of the various prosthetic components in the restorative complex.[6,7] Biologic complications can also manifest as adverse tissue reactions, pain, tenderness, marginal bone loss, and loss of osseointegration.[8] These complications have been

[1]Faculty of Dentistry, National University of Singapore, Singapore, Republic of Singapore.
[2]Associate Consultant, Khoo Teck Puat Hospital, Singapore, Republic of Singapore.

Correspondence to: Prof Eunice Siew Pei Lua, denspel@nus.edu.sg

Submitted December 3, 2024; accepted January 23, 2025.

well-documented in long-term follow-up studies of implant-supported prostheses.[9]

Advancements in CAD/CAM manufacturing technology, including computer-numeric controlled milling techniques, has expanded the technical possibilities to include implant FAFDPs and has allowed for various stages of the conventional workflow to be bypassed. In addition, rising costs of high-noble and noble alloys has seen a shift in interest towards alternative materials like titanium, cobalt-chromium, and zirconia (Zr).

While digital technology appears to provide much-anticipated technical, clinical, and procedural benefits, a recent consensus conference highlighted the scarcity of appropriate clinical documentation to support widespread use of CAD/CAM technology in implant reconstructions.[10] To date, literature on the accuracy of implant prosthodontic procedures has mostly focused up to the impression stage. Several studies have attempted to determine the distortion at the end of the fabrication workflow, but comparisons between studies could not be made due to heterogenous study designs. Many of these studies[5,11,12] also used the superimposition method for distortion analysis and lacked information on inter-implant distances.

The purpose of this study was to quantify and compare the 3D accuracy of conventional cast noble-alloy implant FAFDP frameworks derived via a conventional workflow with milled Zr implant FAFDP frameworks from a digital workflow. The null hypothesis was that no difference in the 3D accuracy of implant FAFDP frameworks would be found regardless of fabrication workflow.

MATERIALS AND METHODS

The master model was fabricated with heat-polymerized polymethyl methacrylate (PMMA) (Lucitone 199 Denture Base Resin, Dentsply Sirona) to simulate a patient with a completely edentulous mandible who needs to be rehabilitated with a mandibular FAFDP supported by five implants (Bone Level Implant [RC 4.8 mm in diameter and 12.0 mm in length], Straumann) approximately 15 mm apart.

A single conventional impression was made of the master model using polyether impression material (Impregum, 3M), dispensed from a Pentamix Automatic Mixing Unit (3M ESPE) and using a custom tray made from auto polymerizing acrylic resin (Tray Resin II, Shofu). The conventional impression was made via the open-tray impression technique and with a torque application of 15 Ncm[13–15] to the impression copings (RC Impression Post 025.4205, Straumann), which were splinted with pattern resin (GC Pattern Resin LS, GC International) incrementally placed on a floss scaffold. To minimize the effect of polymerization shrinkage, the polymerized pattern resin was sectioned between impression copings and small amounts of pattern resin was added to re-attach the segments. Care was taken to prevent rotation of impression copings within the impression material when attaching implant analogs (Bone Level Implant Analog [025.4101], Straumann) to the impression copings, on completion of the conventional impression. A single stone model was poured using type 4 dental stone (Silky Rock, Whip Mix), following the manufacturer's recommended powder to water ratio; this was removed from the impression after 1 hour, and stored at 20 °C for at least 24 hours to mitigate the effects of dental stone expansion. This stone model served as the working model that five conventional noble metal frameworks were fabricated from.

Scan bodies (Cares [025.4915], Straumann) were secured with 10 Ncm[16] of torque to the implant analogs in the working model. A laboratory scan of the working model was done using a dental laboratory scanner (DLS) (D2000, 3Shape) to produce a single virtual model. A DLS was selected due to a lack of established consensus on the use of intraoral scanners (IOS) for full-arch implant rehabilitations.[15,16] Several studies[1,17] have reported superior precision of DLS compared to IOS, with this attributed differences in image acquisition techniques[18,19] and factors that can negatively influence IOS accuracy including space limitations, scanning protocols, and the operator's skills.[20,21] Lack of characteristic reference points and anatomical landmarks in an edentulous arch often results in difficulty in stitching captured images; this problem is significant with IOS due to the IOS image sizes being much smaller than those from DLS.[22,23]

A total of 15 test frameworks were derived from 3 test groups. For the digital fabrication workflow, two designs of implant FAFDP frameworks were created: *(1)* a Zr full-contour design (ZFC) that simulates a monolithic framework with fully contoured tooth segments and only a cutback of the gingival areas, and *(2)* a Zr cutback design (ZCB) that simulates cutback at the buccal areas of posterior teeth, buccoincisal regions of anterior teeth, and the gingival areas (Fig 1). The frameworks incorporated channels to allow for subsequent attachment of abutments. Each channel was designed with a flat surface that corresponds to the flat surface of the abutment, which allowed for accurate seating of abutments. Five of each design were milled in 3Y-TZP Zr (Ceramill Zi, Amann Girrbach) and sintered in the furnace according to manufacturer's recommendations. Variobase cementable abutments were individually cemented onto the Zr framework with a dual-cure resin cement (Multilink N, Ivoclar). This allowed for the quantification of framework distortion only.

Five conventional noble frameworks (CNB) were fabricated by a single technician with two decades of experience in conventional prosthodontic laboratory work. For each pattern, casting wax was milled based on the ZCB digital design to achieve standardization in framework contour and bulk. The milled casting wax was sealed with heated wax to abutments (Regular Connection Gold Abutment for Bridge 022.4430; Straumann) attached to the implant analogs in the working model with a torque application of 10 Ncm. Each wax pattern was left on the working model for 24 hours to allow for stress relaxation. The pattern was checked for accuracy before sprue attachment. Each sprued pattern was left screwed onto the working model for at least 30 minutes before investment. All frameworks were cast in a palladium-silver noble alloy (Argelite 61, Argen), comprising 60.55% of palladium, 28.10% of silver, 6.60% of indium, 2.50% of tin, 2.10% of gallium, and < 1.00% of ruthenium. Each casting used 85 g of alloy.

Implants were attached to the 15 test frameworks with 35 Ncm torque application. These were then set in type 4 dental stone that was vacuum mixed for 30 seconds, according to the manufacturer's recommended powder to water ratio, to derive 15 test models. The test models were stored at 20 °C for at least 24 hours before removing the test frameworks.

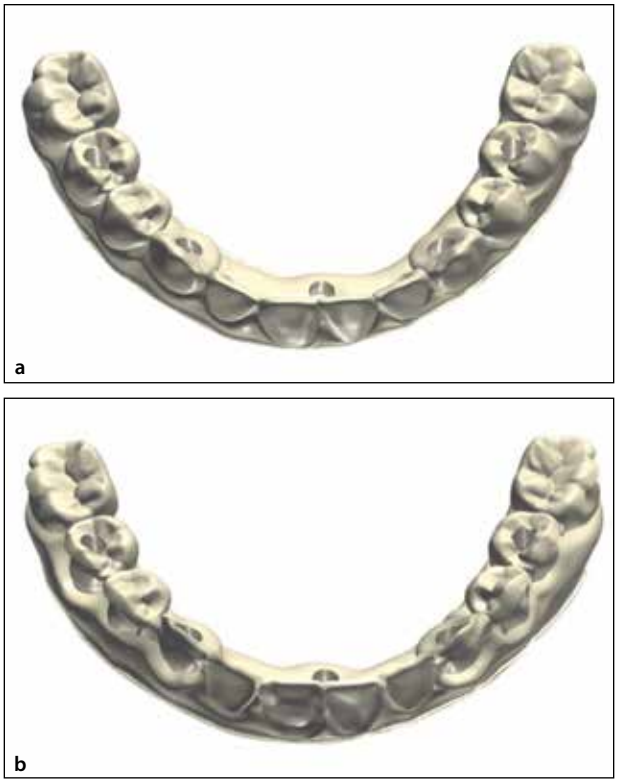

Fig 1 Two digitally fabricated designs of FADP frameworks: *(a)* ZFC design and *(b)* ZCB design.

Coordinate Measuring Machine: Master and Test Model Measurements

Implant positions were determined by a coordinate measuring machine (CMM) with manufacturer-specified accuracy of 2 µm, and its associated metrology software (PC-DMIS CAD ++ 2021, Hexagon). The physical master model, working model, and 15 test models were measured with the CMM spring-loaded ruby ball stylus that were 1.0 mm in diameter and 20.0 mm in shank length (Renishaw). For these physical models, the internal conical portion was measured via ten probe hits to define a plane, while the internal conical portion was measured via 10 probe hits at two levels to define a cone. Each centroid was found by constructing a pierce point between the central axis of the internal cone and the coronal flat plane.

The single virtual model derived from the dental laboratory scanner was exported as a Standard Tessellation Language (STL) file and imported into the same CMM metrology software. The coronal platform of each virtual scan body was measured via four virtual probe hits to define a plane, while the axial portion of each scan body was measured via eight virtual probe hits at two levels to define a cylinder. Each virtual implant centroid was defined by constructing a pierce point between the central axis of the virtual body cylinder and a constructed plane offset by 8.94 mm, which is the height of the scan body.[16]

Each geometric feature was measured three times to minimize the magnitude of errors. A verification check using the CMM software tolerance criterion function was conducted. The tolerance value for all physical geometric features was set at 6 µm, while that for virtual geometric features was set at 20 µm. The higher tolerance limit for the virtual model served to compensate for surface irregularities inherent in STL files without negatively impacting measurement validity. For both physical and virtual models, 3D distances between the three centroids of the same constructed feature were calculated, and a limit of acceptable deviation was set at 10 µm, as established in a similar methodology by Tan et al.[17]

The alignment setup for the models was a local coordinate system that comprised of the centroid of implant A as the origin; implants A, C and E as the *xy*-plane; and implants A and E as the *x*-axis (Fig 2).

Distortion Parameters

Distortion values were derived by calculating the differences in 3D coordinate values between master and test models. Three linear distortions (d_x, d_y, d_z) were computed for each implant, indicating distortion along the

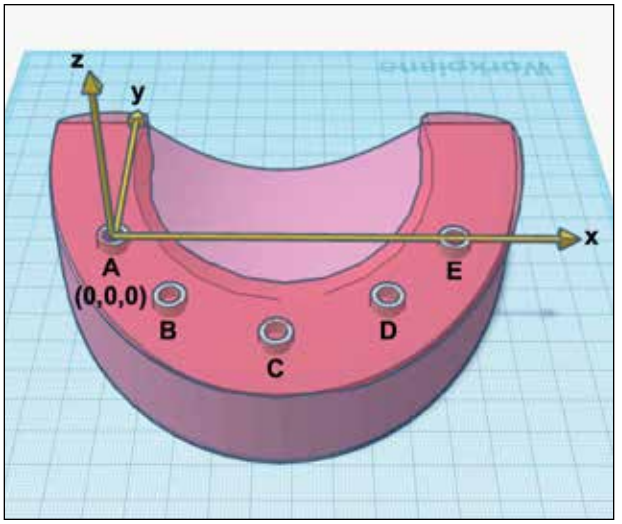

Fig 2 Alignment setup for the measurement protocol of test models.

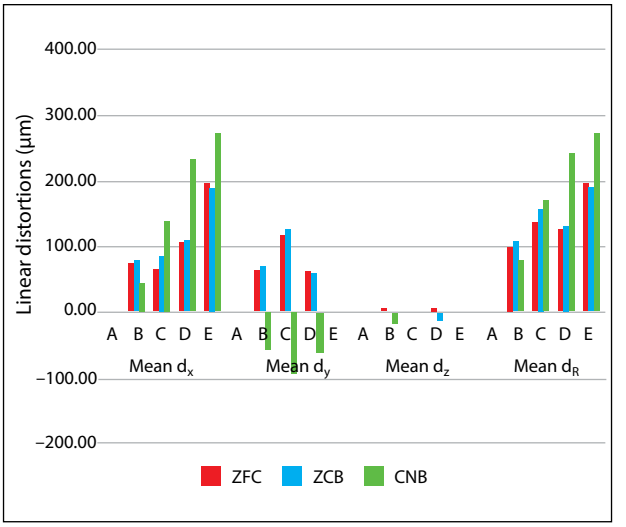

Fig 3 Graph showing 3D and global linear distortions (μm) by implant location.

Table 1 Global Linear (d_R), Angular ($d\theta_x$, $d\theta_y$), and 3D Reference Distance (ΔR) Distortions by Implant Location in Each Model Group

Variable	ZFC, mean (SD)	ZCB, mean (SD)	CNB, mean (SD)
d_R (μm)			
A	0.0 (0.0)	0.0 (0.0)	0.0 (0.0)
B	98.8 (9.5)	107.3 (24.9)	78.1 (32.1)
C	136.0 (16.4)	156.9 (15.6)	169.7 (57.6)
D	125.3 (18.4)	130.5 (18.4)	242.4 (80.5)
E	195.5 (21.4)	189.2 (27.9)	272.3 (94.6)
$d\theta_x$ (degrees)			
A	0.275 (0.325)	0.182 (0.594)	0.256 (0.387)
B	0.480 (0.127)	0.407 (0.319)	0.560 (0.283)
C	0.665 (0.485)	0.323 (0.684)	0.824 (0.383)
D	0.324 (0.383)	0.099 (1.205)	0.557 (0.307)
E	0.983 (0.472)	0.636 (0.435)	0.062 (0.224)
$d\theta_y$ (degrees)			
A	0.774 (0.373)	1.118 (0.464)	0.404 (0.506)
B	0.097 (0.261)	0.146 (0.178)	0.508 (0.125)
C	0.479 (0.449)	0.172 (0.649)	0.300 (0.216)
D	0.063 (0.217)	0.358 (0.378)	0.540 (0.184)
E	0.499 (0.324)	0.812 (0.291)	0.537 (0.392)
ΔR (μm)			
A to B	6.1 (7.7)	4.9 (12.7)	72.4 (32.9)
A to C	4.6 (24.0)	8.4 (39.7)	171.3 (57.8)
A to D	84.6 (19.4)	89.4 (24.3)	240.5 (81.3)
A to E	195.5 (21.4)	189.2 (27.9)	272.3 (94.6)

x-, *y*-, and *z*-axes, respectively. *Global linear distortion* (d_R) was defined by the following formula:

$$d_R = \sqrt{(d_x^2 + d_y^2 + d_z^2)}$$

Two angles (θ_x, θ_y) about the *x*- and *y*-axes respectively were computed. The angular distortion $d\theta_x$ reflected angular distortions of implants in the anteroposterior dimension, while $d\theta_y$ reflected angular distortions of implants in the mediolateral dimension.

3D reference distances (R) between implant in the test models were compared to those in the master models to derive 3D reference distance distortions (ΔR).

The dependent variables were d_x, d_y, d_z, d_R, $d\theta_x$, $d\theta_y$, and ΔR. One-way ANOVA and post-hoc Tukey honestly significant difference (HSD) tests were used for the comparison of the framework design. Significance was reported at a level of $\alpha = .05$. All statistical calculations were performed using statistical software (SPSS Statistics v28.0.1.1, IBM).

RESULTS

The 3D linear distortions (d_x, d_y, d_z) as well as the global linear distortion (d_R) are shown in Fig 3 and Table 1. The magnitude of mean d_R ranged from 78.1 ± 32.1 μm in CNB to 107.3 ± 24.9 μm in ZCB for implant B; 136.0 ± 16.4 μm in ZFC to 169.7 ± 57.6 μm in CNB for implant C; 125.3 ± 18.3 μm in ZFC to 242.4 ± 80.5 μm in CNB for implant D; and 189.2 ± 27.9 μm in ZCB to 272.3 ± 94.6 μm in CNB for implant E.

The angular distortions ($d\theta_x$, $d\theta_y$) are shown in Fig 4 and Table 1. The magnitude of mean $d\theta_x$ ranged from

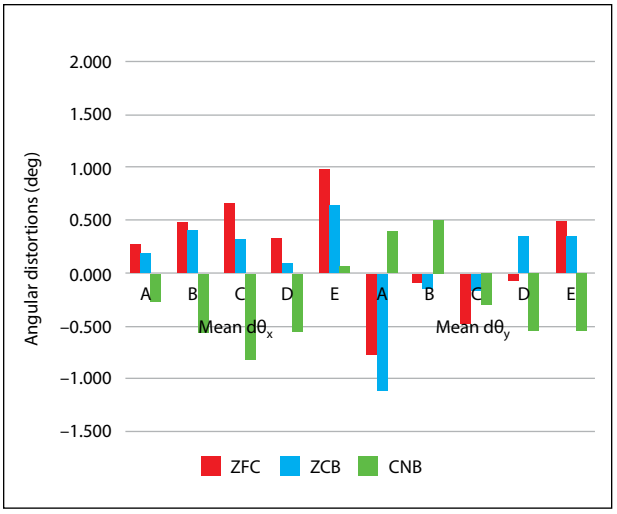

Fig 4 Graph showing angular distortions (degrees) by implant location.

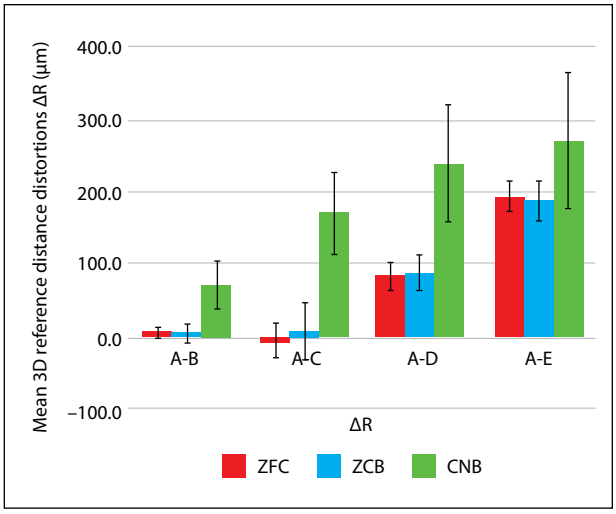

Fig 5 Graph showing mean 3D reference distance distortions (μm) by implant distance.

0.182 ± 0.594 degrees in ZCB to 0.275 ± 0.325 degrees in ZFC for implant A; 0.407 ± 0.319 degrees in ZCB to −0.560 ± 0.283 degrees in CNB for implant B; 0.323 ± 0.684 degrees in ZCB to −0.824 ± 0.383 degrees in CNB for implant C; 0.099 ± 1.205 degrees in ZCB to −0.557 ± 0.307 degrees in CNB for implant D; and 0.062 ± 0.224 degrees in CNB to 0.983 ± 0.472 degrees in ZFC for implant E. The magnitude of mean for $d\theta_y$ ranged from 0.404 ± 0.506 degrees in CNB to −1.118 ± 0.464 degrees in ZCB for implant A; −0.097 ± 0.261 degrees in ZFC to 0.508 ± 0.125 degrees in CNB for implant B; −0.172 ± 0.649 degrees in ZCB to −0.479 ± 0.449 degrees in ZFC for implant C; −0.063 ± 0.217 degrees in ZFC to −0.540 ± 0.184 degrees in CNB for implant D; and 0.499 ± 0.324 degrees in ZFC to 0.812 ± 0.291 degrees in ZCB for implant E.

Mean 3D reference distance distortions (ΔR) are shown in Fig 5 and Table 1. The magnitude of mean ΔR ranged from 4.9 ± 12.7 μm in ZCB to 72.4 ± 32.9 μm in CNB for reference distance A to B; −4.6 ± 24.0 μm in ZFC to 171.3 ± 57.8 μm in CNB for reference distance A to C; 84.6 ± 19.4 μm in ZFC to 240.5 ± 81.3 μm in CNB for reference distance A to D; 189.2 ± 27.9 μm in ZCB to 272.3 ± 94.6 μm in CNB for reference distance A to E.

The data were initially submitted to the Shapiro-Wilk test to check for the assumption of normality and it was not rejected. One-way ANOVA by fabrication group revealed significant differences among the test groups for d_x, d_y, d_z, $d\theta_x$, and $d\theta_y$ at some implant locations, but there was no clear pattern on the poorest group. For the global linear distortion d_R, statistical difference was found at implant D, where CNB fared the worst. CNB exhibited the worst accuracy in ΔR for all reference distances except A to E. Tables 2 and 3 summarize the results of the one-way ANOVA and Tukey HSD procedures performed.

DISCUSSION

Accuracy of the working model and virtual model were verified by comparing against the master model. For the working model, d_R ranged from 2.0 μm to 14.4 μm and ΔR ranged from −0.3 μm to 7 μm; these values indicate the cumulative distortion associated with conventional polyether impression making and subsequent model fabrication using type 4 dental stone. For the virtual model, d_R ranged from 14.1 μm to 25.0 μm and ΔR ranged from 5.7 μm to 25 μm; these values indicate the cumulative distortion associated with conventional polyether impression making, model fabrication using type 4 dental stone, and scans with a DLS. These results were comparable to Tan et al,[17] which used a similar CMM measurement protocol.

The present study's results do not support the null hypothesis. Compared to Zr frameworks, noble alloy frameworks fabricated by the conventional workflow fared poorer for ΔR for three of four reference distances, as well as for dR for one of five implant positions (implant D). There was no significant difference in 3D accuracy between the Zr groups.

Linear Distortions

The investigated fabrication methods could not be consistently ranked for linear distortions. Linear distortions in the x-direction (d_x) for all implants across the three groups were consistently positive, indicating expansion in the width of the framework. For d_y, CNB

Table 2 Summary of One-Way ANOVA and Tukey HSD Analyses of Global (d_R), Linear (d_x, d_y, and d_z), and Absolute Angular Distortions ($d\theta_x$ and $d\theta_y$) by Implant Location in Each Model Group

Variable	Statistically significant subsets			
	P	ZFC	ZCB	CNB
d_x				
A	—	—	—	—
B	.044	a	a	a
C	.022	a	a,b	b
D	.003	a	a	b
E	.079	a	a	a
d_y				
A	—	—	—	—
B	.000	a	a	b
C	.000	a	a	b
D	.000	a	a	b
E	—	—	—	—
d_z				
A	—	—	—	—
B	.075	a	a	a
C	—	—	—	—
D	.402	a	a	a
E	—	—	—	—
d_R				
A	—	—	—	—
B	.187	a	a	a
C	.355	a	a	a
D	.004	a	a	b
E	.079	a	a	a
$d\theta_x$				
A	.180	a	a	a
B	.000	a	a	b
C	.002	a	a	b
D	.199	a	a	a
E	.009	a	a,b	b
$d\theta_y$				
A	.000	a	a	b
B	.000	a	a	b
C	.600	a	a	a
D	.000	a	a	b
E	.000	a	a	b

Letters *a* and *b* indicate results of statistical analyses; variables with different letters are significantly different ($P < .05$).

Table 3 Summary of One-Way ANOVA and Tukey HSD for 3D Reference Distance (ΔR) Distortions

Implant reference distance	Statistically significant subsets			
	P	ZFC	ZCB	CNB
ΔR				
A to B	.000	a	a	b
A to C	.000	a	a	b
A to D	.000	a	a	b
A to E	.079	a	a	a

Letters *a* and *b* indicate results of statistical analyses; implant reference distances with different letters are significantly different ($P < .05$).

was consistently negative, whereas both Zr groups were consistently positive, indicating shrinkage for CNB frameworks and expansion for ZFC and ZCB frameworks in the anteroposterior dimension. Linear distortions in the z-direction (d_z) did not demonstrate a trend of being consistently positive or negative across all three groups, and there was no observable relationship with implant location. These results suggest that the digital workflow tends to produce frameworks that are larger in both mediolateral and anteroposterior dimensions. On the other hand, the conventional workflow tends to produce frameworks that are larger in the mediolateral dimension but smaller in the anteroposterior dimension.

A general trend of increasing global linear distortion (d_R) was observed with increasing implant distance from implant A, the origin. CNB exhibited the largest range of d_R, while ZFC and ZCB showed relatively smaller ranges of d_R. This suggests that the global linear distortion of digitally fabricated Zr frameworks may fall within a narrower range of error, in turn producing more precise restorations compared to conventionally fabricated frameworks.

Angular Distortions and 3D Reference Distance Distortions

The test groups could not be consistently ranked for angular distortions regarding the *x*- and *y*-axes. There were no significant differences between ZFC and ZCB for $d\theta_x$ and $d\theta_y$ at all implant locations. ZFC and ZCB groups did not exhibit observable patterns of angular distortions about the *x*- and *y*-axes, which could be attributed to the lack of predictability in the direction of distortion as part of the sintering process of Zr frameworks.

On the contrary, CNB demonstrated a trend of increasingly negative $d\theta_x$ values from implant A to C, which gradually decreased in value from implant C to E, with implant E having a positive mean value. The $d\theta_y$ values for implants A and B in CNB were positive and negative for implant C to E. The pattern of angular distortion of the *x*- and *y*-axes for CNB is consistent with the conventional method of the lost-wax technique, with shrinkage towards the sprue.[18]

CNB performed significantly poorer for all 3D reference distance distortions (ΔR), except for the 3D reference distance of A to E, which did not reach statistical significance.

Comparison with Previous Studies

Tan et al[18] investigated the 3D accuracy of two different designs of one-piece implant supported FAFDP cast frameworks using a similar measurement methodology to the present study[19–21]; however, the studies differed in terms of framework dimensions, as the frameworks in the present study had larger arch widths and narrower arch heights. The conventional cast frameworks in both studies did not demonstrate any consistent pattern of distortion in the z-direction, which affects the abutment heights of the implants relative to each other. Both studies revealed a trend of increasing d_R with increasing implant distance from the origin. Lastly, the pattern of distortion of the conventional cast frameworks was found to be similar to that reported by Tan et al.[18]

Limitations

The in vitro nature of this study eliminated several patient- and operator-related factors that could have affected results. The conventional impression was made on a master model with no surrounding saliva, soft tissue, and oral musculature, which allowed optimal access and visibility over the procedure. In addition, parallel implants were chosen over angulated ones, which have been reported to affect impression and scan accuracies.[14] This allowed for a reduction of experimental variables in this study, thus focusing on the influence of fabrication technique on accuracy of the framework. However, in a clinical situation, it is likely that implants will be angulated, and this should be further investigated in future studies.

The use of a DLS may appear to contrast with clinical reality where clinicians who choose to use an IOS can overcome the need for a conventional impression. While clinical utility of IOS has certainly increased in recent years, a conventional impression coupled with DLS was selected for this study, resulting in a partially digital workflow for the fabrication of Zr FAFDPs. This decision was due to a lack of established consensus on the use of IOS for full-arch implant rehabilitations.[22,23] Furthermore, the conventional impression procedure, which utilizes elastomeric impression materials and splinted implant impression copings, has been regarded as a gold standard for comparison with the accuracy of various scanners. Several studies[1,17] have also reported superior precision of DLS compared to IOS, with this attributed to differences in image acquisition techniques[3,24] and factors that can negatively influence IOS accuracy including space limitations, scanning protocol, and the operator's skills.[25,26] Lack of characteristic reference points and anatomical landmarks in an edentulous arch often results in difficulty in stitching captured images; this problem is significant with IOS due to the IOS image sizes being much smaller than those from DLS.[25,27]

Alternative software are available to determine implant positions via a "best-fit" algorithm and have become increasingly popular. Unfortunately, such methods require additional scans and may introduce confounding errors. The accuracy of these software algorithms also cannot be evaluated as the process of data manipulation are proprietary to the manufacturer and are not reported. Therefore, the present study used CMM metrology for the determination of implant centroids. It is acknowledged that measurement accuracy for each geometric feature is dependent on the proper execution of probe hits, selection of an optimal number of probe hits, and careful selection of sites for these probe hits. This measurement method is technique sensitive and required significant operator training. Strict tolerance criteria were implemented to ensure measurement accuracy.

The present study compared 3D accuracy of implant FAFDP frameworks produced from conventional and digital workflows. The five conventional frameworks were casted as single-pieces to demonstrate the potential magnitude of distortion without further fit improvement techniques. In reality, single-piece casted conventional frameworks often require adjustment procedures to improve fit, including sectioning and soldering. An alternative method is to cast the framework in several pieces and solder the pieces together. Future studies could look at the accuracy of the conventional framework after such fit adjustment procedures.

CONCLUSIONS

This in vitro study compared 3D accuracy of conventional and digital workflows in the fabrication of implant full-arch fixed dental prosthesis (FAFDP) frameworks for an edentulous mandible. Within the limitations of this study, the following conclusions were made:

1. There was no difference between ZFC and ZCB for all parameters.
2. CNB fared poorest for ΔR for three of four reference distances (A-B, A-C, and A-D), as well as for dR for one of five implant locations (implant D).

ACKNOWLEDGMENTS

This study was supported by the Ministry of Education Academic Research Fund (Tier 1) (WBS R-221-000-155-114) and the National University of Singapore, Master of Dental Surgery (MDS) Research Grant. The authors thank Mr Timan Eduardo Llanto Jr and Mr Joseph Xu Weijian for technical assistance. The authors reported no conflicts of interest related to this study.

This paper was presented in an ePoster presentation at the Academy of Osseointegration's Annual Meeting in 2024.

REFERENCES

1. Flügge TV, Att W, Metzger MC, Nelson K. Precision of dental implant digitization using intraoral scanners. Int J Prosthodont 2016;29:277–283.
2. Spazzin AO, Henrique GE, Nóbilo MA, Consani RL, Correr-Sobrinho L, Mesquita MF. Effect of retorque on loosening torque of prosthetic screws under two levels of fit of implant-supported dentures. Braz Dent J 2010;21:12–17.
3. Alsharbaty MHM, Alikhasi M, Zarrati S, Shamshiri AR. A clinical comparative study of 3-dimensional accuracy between digital and conventional implant impression techniques. J Prosthodont 2019;28:902–908.
4. Assif D, Fenton A, Zarb G, Schmitt A. Comparative accuracy of implant impression procedures. Int J Periodontics Restorative Dent 1992;12:112–121.
5. Paniz G, Stellini E, Meneghello R, Cerardi A, Gobbato EA, Bressan E. The precision of fit of cast and milled full-arch implant-supported restorations. Int J Oral Maxillofac Implants 2013;28:687–693.
6. Sahin S, Cehreli MC. The significance of passive framework fit in implant prosthodontics: Current status. Implant Dent 2001;10:85–92.
7. Sones AD. Complications with osseointegrated implants. J Prosthet Dent 1989;62:581–585.
8. Adell R, Eriksson B, Lekholm U, Brånemark PI, Jemt T. Long-term follow-up study of osseointegrated implants in the treatment of totally edentulous jaws. Int J Oral Maxillofac Implants 1990;5:347–359.
9. Tan KB. The clinical significance of distortion in implant prosthodontics: Is there such a thing as passive fit? Ann Acad Med Singap 1995;24:138–157.
10. Hämmerle CH, Cordaro L, van Assche N, et al. Digital technologies to support planning, treatment, and fabrication processes and outcome assessments in implant dentistry. Summary and consensus statements. The 4th EAO consensus conference 2015. Clin Oral Implants Res 2015;26(suppl 11):S97–S101.
11. Al-Fadda SA, Zarb GA, Finer Y. A comparison of the accuracy of fit of 2 methods for fabricating implant-prosthodontic frameworks. Int J Prosthodont 2007;20:125–131.
12. Ortorp A, Jemt T, Bäck T, Jälevik T. Comparisons of precision of fit between cast and CNC-milled titanium implant frameworks for the edentulous mandible. Int J Prosthodont 2003;16:194–200.
13. Chew AA, Esguerra RJ, Teoh KH, Wong KM, Ng SD, Tan KB. Three-dimensional accuracy of digital implant impressions: Effects of different scanners and implant level. Int J Oral Maxillofac Implants 2017;32:70–80.
14. Chia VA, Esguerra RJ, Teoh KH, Teo JW, Wong KM, Tan KB. In vitro three-dimensional accuracy of digital implant impressions: The effect of implant angulation. Int J Oral Maxillofac Implants 2017;32:313–321.
15. Teo JW, Tan KB, Nicholls JI, Wong KM, Uy J. Three-dimensional accuracy of plastic transfer impression copings for three implant systems. Int J Oral Maxillofac Implants 2014;29:577–584.
16. Tan JZH, Tan MY, See Toh YL, Wong KY, Tan KBC. Three-dimensional positional accuracy of intraoral and laboratory implant scan bodies. J Prosthet Dent 2022;128:735–744.
17. Tan MY, Yee SHX, Wong KM, Tan YH, Tan KBC. Comparison of three-dimensional accuracy of digital and conventional implant impressions: Effect of interimplant distance in an edentulous arch. Int J Oral Maxillofac Implants 2019;34:366–380.
18. Tan KB, Rubenstein JE, Nicholls JI, Yuodelis RA. Three-dimensional analysis of the casting accuracy of one-piece, osseointegrated implant-retained prostheses. Int J Prosthodont 1993;6:346–363.
19. Nicholls JI. The measurement of distortion: theoretical considerations. J Prosthet Dent 1977;37:578–586.
20. Nicholls JI. The measurement of distortion: Mathematical considerations. J Prosthet Dent 1978;39:339–343.
21. Nicholls JL. The measurement of distortion: Concluding remarks. J Prosthet Dent 1980;43:218–223.
22. Papaspyridakos P, Chen CJ, Gallucci GO, Doukoudakis A, Weber HP, Chronopoulos V. Accuracy of implant impressions for partially and completely edentulous patients: A systematic review. Int J Oral Maxillofac Implants 2014;29:836–845.
23. Revilla-León M, Att W, Özcan M, Rubenstein J. Comparison of conventional, photogrammetry, and intraoral scanning accuracy of complete-arch implant impression procedures evaluated with a coordinate measuring machine. J Prosthet Dent 2021;125:470–478.
24. Gherlone EF, Ferrini F, Crespi R, Gastaldi G, Capparé P. Digital impressions for fabrication of definitive "all-on-four" restorations. Implant Dent 2015;24:125–129.
25. Sallorenzo A, Gómez-Polo M. Comparative study of the accuracy of an implant intraoral scanner and that of a conventional intraoral scanner for complete-arch fixed dental prostheses. J Prosthet Dent 2022;128:1009–1016.
26. Michelinakis G, Apostolakis D, Kamposiora P, Papavasiliou G, Özcan M. The direct digital workflow in fixed implant prosthodontics: A narrative review. BMC Oral Health 2021;21:37.
27. Uribarri A, Bilbao-Uriarte E, Segurola A, Ugarte D, Verdugo F. Marginal and internal fit of CAD/CAM frameworks in multiple implant-supported restorations: Scanning and milling error analysis. Clin Implant Dent Relat Res 2019;21:1062–1072.